Polyoxometalates

DOI: 10.1002/ange.200805323

Direct Observation of Contact Ion-Pair Formation in Aqueous Solution**

Mark R. Antonio, May Nyman,* and Travis M. Anderson*

The formation of ion pairs in aqueous solution orchestrates vital processes in nature and engineered systems, including electron transfer[1–3] and other chemical reactions,[4,5] and crystallization/precipitation of synthetic and natural matter.[6–9] Polyoxometalates (POMs) have received special attention with regard to ion pairing.[10] POMs are highly charged anions with ideal topologies for binding and associating metal cations, as their assembly,[11–13] redox,[2] and catalytic properties[14] in aqueous solution are influenced by ion pairing. Methods for determining ion pairing[15] are largely considered to be indirect in that they observe physical changes in a solution that results from ion association. Spectroscopic methods are the exception, but these are prone to insufficient resolution, and are unable to detect solvent-separated ion pairing. Herein we show that small-angle X-ray scattering (SAXS) of the Lindqvist $[Nb_6O_{19}]^{8-}$ POM[16,17] provides a model example of direct measurement of the formation of ion pairs in aqueous solution, and reveals remarkable similarity between solution and solid-state ion contact. This study provides evidence that the structures of Lindqvist hexaniobate salts described with extreme accuracy in the solid state can be used to model the ion-pairing behavior in solution.

The effectively spherical $[Nb_6O_{19}]^{8-}$ isopolyoxoanion with 25 atoms (Figure 1a) has the greatest surface charge of all POMs.[18] High surface charge is a property noted to enhance ion pairing, both in solution[2] and in the resulting precipitates.[19] In fact, niobates are unique amongst POMs in that their behavior is controlled by high surface charge. They form similar cluster geometries as the tungstate POMs, most notably the α-Keggin ion and its derivatives, although the charges differ considerably; that is, $[SiNb_{12}O_{40}]^{16-}$ versus $[SiW_{12}O_{40}]^{4-}$. Thus, compared to tungstate, molybdate, and vanadate POMs, niobate POMs are not electrochemically reducible, they are assembled and stabilized in alkaline rather than acidic solutions,[20] they protonate rather than deprotonate in water,[21] and tend to form insoluble linked frameworks with alkali atoms[22,23] rather than soluble salts.

The $[Nb_6O_{19}]^{8-}$ Lindqvist ion has been crystallized in the solid state with every alkali metal counterion,[24–26] and its ion

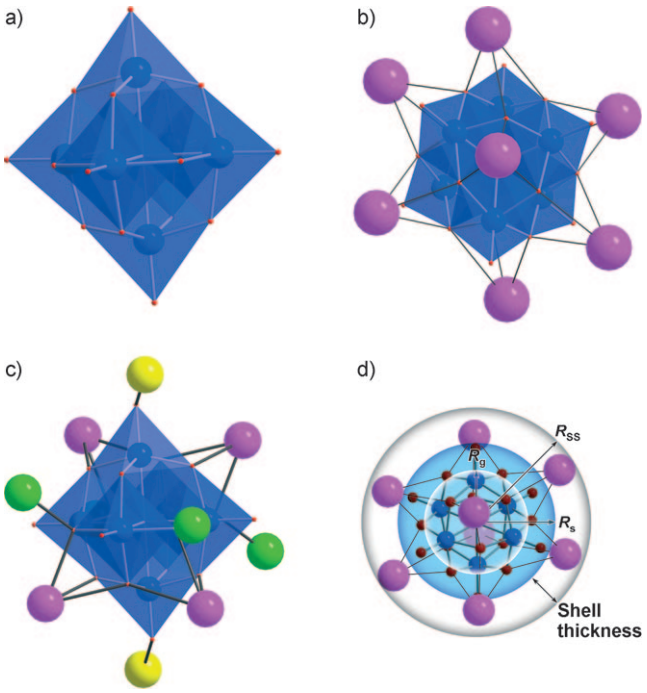

Figure 1. a) The bare $[Nb_6O_{19}]^{8-}$ Lindqvist ion. Blue octahedra are NbO_6. b) The neutral $A_8[Nb_6O_{19}]$ species (A = Rb, Cs). Pink spheres are face-bonded Rb/Cs^+. c) K^+–$[Nb_6O_{19}]^{8-}$ association observed in the crystal structure. Spheres indicate K^+ associated on the cluster face (pink), cluster edge (green), and cluster apices (yellow). d) Representation of the three particle radii (R_g, R_S, and R_{SS}) obtained from the analysis of the SAXS data and utilizing the $A_8[Nb_6O_{19}]$ species from Figure 1b. The radius of gyration, R_g (inner white sphere), for the randomly-orientated, rotationally-averaged blue middle sphere of the bare $[Nb_6O_{19}]^{8-}$ ion is related to its physical radius R_S (blue sphere radius) by the relationship $R_S = \sqrt{\frac{5}{3}}R_g$. All the R_S values presented in Table 2 were obtained directly from fitting the SAXS data with a spherical form factor model. The R_{SS} (spherical shell radius; represented by the outermost white sphere) is the sum of the physical radius of the bare anion (fixed at 3.9 Å) and the best-fit thickness of the spherical shell around the hexaniobate core.

[*] Dr. M. R. Antonio
Chemical Sciences and Engineering Division, Argonne National Laboratory, Argonne, IL 60439-4831 (USA)
E-mail: mantonio@anl.gov
Homepage: http://www.cse.anl.gov/Staff/Nuclear_and_Environmental_Processes/MAntonio.shtml
Dr. M. Nyman, Dr. T. M. Anderson
Geochemistry Department, Sandia National Laboratories
Albuquerque, NM 87185-0754 (USA)
E-mail: mdnyman@sandia.gov

[**] We thank Dr. Soenke Seifert (XSD-APS-ANL) for assistance with the SAXS measurements and Dr. Nate Ockwig for assistance in data collection. This work is supported by the U. S. Department of Energy, Office of Basic Energy Science, Division of Chemical Sciences, Biosciences and Geosciences, under contract no. DE-AC02-06CH11357, for the part performed at Argonne National Laboratory. We are grateful to Mona Aragon (SNL) for assistance with graphics. Sandia authors thank the LDRD program for financial support. Sandia is a multiprogram laboratory operated by Sandia Corporation, a Lockheed-Martin Company, for the United States Department of Energy under Contract No. DE-AC04-94AL85000.

Supporting information for this article is available on the WWW under http://dx.doi.org/10.1002/anie.200805323.

association in the crystal lattice with the alkali counterions increases with alkali size.[26] A particularly favorable ion-association motif is one in which the alkali ion associates on the super-octahedral faces through three bonds to cluster (bridging) oxygen atoms; and there is a distinct trend with the size of the alkali atom for which the order of decreasing ion association is Cs = Rb > K > Na = Li. Rubidium and cesium salts of $[Nb_6O_{19}]^{8-}$ (Figure 1b) associate with eight alkali metal ions, one on each face of the superoctahedron, described as the neutral molecule $A_8[Nb_6O_{19}]$ (A = Rb, Cs). The $[Nb_6O_{19}]^{8-}$ Lindqvist ion of the potassium salt can host four of these face-bonded potassium ions, forming $K_4[Nb_6O_{19}]^{4-}$. Four additional potassium ions can be singly bonded to the edge of the superoctahedron to form $K_8[Nb_6O_{19}]$, and two more potassium ions singly bonded to the apices of the superoctahedron forms $K_{10}[Nb_6O_{19}]^{2+}$ (Figure 1c). If the ion association between the A^+ ion (A = K, Rb, Cs) and $[Nb_6O_{19}]^{8-}$is retained in aqueous solution, these highly symmetric, effectively spherical structures coupled with excellent X-ray scattering nuclei would provide an ideal case study for accurate ion-pairing observations. Furthermore, whereas the solubility of classical POMs, such as polytungstates decreases significantly with increasing alkali radii,[27] the trend is uniquely opposite for alkali metal salts of $[Nb_6O_{19}]^{8-}$. This unprecedented characteristic also renders the system of $A_8[Nb_6O_{19}]$ salts optimal for the present study: maximum solubility, maximum ion-pair formation, and maximum X-ray scattering can be achieved simultaneously from the rubidium and the cesium salts. The results of our calculations on the atomic small-angle X-ray scattering (SAXS) intensities $I_a(Q)$ versus the magnitude of the scattering vector Q ($Å^{-1}$), from the crystallographically determined atomic coordinates of the rubidium and the cesium salts supports the above hypothesis (Supporting Information, Figure S1). The calculated radius of gyration R_g, which provides a shape-independent, root-mean-square measure of all the mass-weighted distances in a particle from its center of mass[28] for the 25-atom bare cluster anion, $[Nb_6O_{19}]^{8-}$ is 3.0 Å. This value of R_g is independent of the nature of the A^+ ion. The R_g values calculated for the 33-atom $8\,A^+$ ion-paired neutral clusters, $A_8[Nb_6O_{19}]$, are 3.5 and 3.6 Å for A = Rb and Cs, respectively. The R_g values calculated for $K_4[Nb_6O_{19}]^{4-}$, $K_8[Nb_6O_{19}]$, and $K_{10}[Nb_6O_{19}]^{2+}$ are 3.3, 3.6, and 3.8 Å, respectively. Therefore the effect of pairing alkali metal ions with $[Nb_6O_{19}]^{8-}$ ions on R_g is a value that is 0.3–0.8 Å larger than the bare anion. Such differences can be readily resolved by using SAXS as applied to the systems of high-atomic-number atoms examined here (A-Nb-O).

The average experimental value for R_g for each of the three series of solutions of different concentrations of the potassium, rubidium, and cesium $[Nb_6O_{19}]^{8-}$ salts dissolved in 3 M tetramethylammonium hydroxide (TMAOH) solution (Table 1) are 3.1(1) Å (Table 2). This value of R_g is consistent with the value calculated for the bare anion (3.0 Å), and is independent of the concentration of the salts (Figure 2, left panel). Futhermore, there is no evidence for the organized association of tetramethylammonium (TMA) cations (with an effective spherical radius of 2.8 Å[29]) with $[Nb_6O_{19}]^{8-}$ anions. In view of the spherical morphology of the $[Nb_6O_{19}]^{8-}$ anion, the average experimental R_g value of 3.1(1) Å can be used to calculate the average physical radius of the Lindqvist sphere R_S using $R_S = \sqrt{\frac{5}{3}}R_g$, as depicted schematically in Figure 1d.[30] The calculated R_S value of 4.0 Å is consistent with the 4.2 Å radius determined from X-ray diffraction measurements as the average distance between the central oxygen atoms to the six terminal oxygen atoms (apices of the superoctahedron) for the structures illustrated in Figure 1. Furthermore, the isotropic scattering obtained for the randomly oriented, rotationally averaged molecular anions is best modeled with a solid-sphere form factor, which is consistent with scattering particles having a continuous electron density. The fits to the $I(Q)$ data (see Supporting Information, Figure S7–S9) pro-

Table 1: Properties of hydrated alkali cations, and concentrations of $A_8[Nb_6O_{19}]$ Lindqvist ion solutions for SAXS studies.

Solution matrix	3 M TMAOH[a]			3 M AOH (A = K, Rb, Cs)		
A-counterion of Lindqvist salt[a]	K	Rb	Cs	K	Rb	Cs
Ionic radius [Å]	1.52	1.66	1.81	–	–	–
Approximate hydrated radius [Å]	2.32	2.28	2.28	–	–	–
Approximate hydration number	11	10	10	–	–	–
Concentration of	0.56	0.56	0.56	0.56	0.56	0.56
Lindqvist salt [mM]	2.78	2.78	–	2.78	2.78	2.78
	5.56	5.56	5.56	5.56	5.56	5.56
	16.7	16.7	16.7	16.7	16.7	16.7
	55.6	55.6	55.6	55.6	55.6	55.6

Table 2: Guinier analysis of the experimental SAXS data compared to radii calculated from X-ray diffraction data along with radii obtained from the best fits to the experimental SAXS data with form factor models.[a]

	3 M TMAOH						3 M AOH (A = K, Rb, Cs)					
Conc.	K		Rb		Cs		K		Rb		Cs	
[mM]	R_g[b]	R_S	R_g[b]	R_S	R_g[b]	R_S	R_g[b]	R_{SS}	R_g[b]	R_{SS}	R_g[b]	R_{SS}
0.56	3.0	4.0	3.0	4.0	2.9	4.4	3.5	6.9	3.6	6.4	na[c]	
2.78	3.1	4.0	3.1	4.2	np[d]		3.6	6.9	3.6	6.7	3.7	6.3
5.56	3.1	4.2	3.1	4.3	3.1	4.5	3.6	7.7	3.7	5.8	3.7	5.9
16.7	3.1	4.1	3.2	4.4	3.2	4.7	3.7	7.8	3.7	6.3	3.5	5.8
55.6	3.1	4.1	3.2	4.5	3.1	4.8	3.9	8.5	3.6	5.5	3.5	5.6
av.	3.1(1)	4.1(1)	3.1(1)	4.3(2)	3.1(1)	4.6(2)	3.7(2)	7.6(7)	3.6(1)	6.1(5)	3.6(1)	5.9(3)

[a] Shape-independent radius of gyration, R_g, is from the fits of the $\ln(I(Q))$ vs. Q^2 data of Figure S2 and S3 (Supporting Information). Fitting of the primary $I(Q)$ vs. Q data with spherical (Figure S7–S9, Supporting Information) and spherical shell (Figure S11–S13, Supporting Information) form factors provided the sphere radii, R_S and R_{SS}, respectively, which for the latter is the sum of the spherical core radius of $[Nb_6O_{19}]^{8-}$, which was fixed at 3.9 Å, and the best fit thickness of the spherical shell as depicted in Figure 1d. The estimated standard deviations on all R obtained from the Guinier and sphere fits is ±0.1 Å. [b] R_g calculated from single-crystal X-ray diffraction data: $[Nb_6O_{19}]^{8-}$, $Rb_8[Nb_6O_{19}]$, $Cs_8[Nb_6O_{19}]$, $K_4[Nb_6O_{19}]^{4-}$, $K_{10}[Nb_6O_{19}]^{2+}$, and $K_8[Nb_6O_{19}]$ are 3.0, 3.5, 3.6, 3.3, 3.6, and 3.8, respectively (see Figure 1c). [c] na, not available: data vitiated by absorbance effects. [d] np, not prepared.

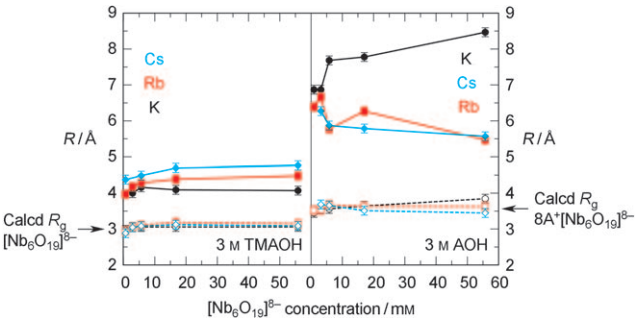

Figure 2. Variation of radii (R_g, R_S, R_{SS}) with solution concentrations of $A_8[Nb_6O_{19}]\cdot x H_2O$ (A = K, ●); Rb (■); Cs (◆) in 3 M TMAOH (left panel) and 3 M AOH (right panel). The Guinier radii of gyration R_g are shown as open symbols connected with dashed lines. The solid sphere radii R_S obtained by fitting the SAXS obtained in 3 M TMAOH with a solid sphere form factor are shown in the left panel as filled symbols connected with solid lines. The spherical shell radii, R_{SS}, obtained by fitting the SAXS obtained in 3 M AOH with a spherical shell form factor are shown in the right panel as filled symbols connected with solid lines. The calculated R_g values for bare $[Nb_6O_{19}]^{8-}$ and $A_8[Nb_6O_{19}]$ are indicated with arrows in the left and right panels, respectively.

vide an independent measure of R_S (Figure 2, left panel). The average R_S of 4.1(1), 4.3(2), and 4.6(2) Å for the K, Rb, and Cs salt solutions, respectively (Table 2) correspond well with the 4.2 Å crystallographic value. The +0.2 to +0.3 Å dispersion of experimental R_S values between potassium/rubidium and rubidium/cesium salt solutions, notably at 55.6 mM (47.9 mg mL^{-1}), is consistent with the increase of ionic radii $K^+ < Rb^+ < Cs^+$ (1.38, 1.52, 1.67 Å for coordination number six),[31] suggesting some extent of alkali metal ion association with the hexaniobate anion at this dilution, even in 3 M TMAOH. At higher concentrations, namely 390 mM and above depending upon solubility, the SAXS data (Supporting Information, Figure S10) demonstrate the presence of larger aggregates of the bare anion and the A^+/TMA^+ counter-cations.

The average experimental R_g values for each of the three series of solution concentrations for the potassium, rubidium, and cesium hexaniobate salts in their corresponding 3 M alkali metal hydroxide (AOH, A = K, Rb, Cs) media (Table 1) are essentially the same, namely 3.6(1)–3.7(2) Å (Table 2). These values are equivalent to the calculated R_g values (3.5–3.6 Å) for the ion-paired, $A_8[Nb_6O_{19}]$ species in the solid state (A = Rb, Cs; Figure 1 b); and those (3.6–3.8 Å) for $K_8[Nb_6O_{19}]$ and $K_{10}[Nb_6O_{19}]^{2+}$ (Figure 1 c). These values are also independent of the concentration of the hexaniobate anion (Figure 2, right panel). Moreover, the average, experimentally-determined R_g values are consistently 0.5–0.6 Å larger than the average, experimental R_g of 3.1(1) Å for the same dilutions of $A_8[Nb_6O_{19}]$ in 3 M TMAOH (Table 2). The agreement between the calculated and experimental results, and the system-wide increase of the R_g values in 3 M AOH (A = K, Rb, Cs) provide direct evidence for contact ion pairing of the hexaniobate isopolyoxoanion with alkali metal ions. Details of the morphology of the solution aggregates were obtained by fitting the scattering intensity $I(Q)$ with a variety of geometrical form-factor models. For all three systems in 3 M AOH (A = K, Rb, Cs), the best fits (Supporting Information, Figure S11–S13) were obtained with a spherical shell form factor model (R_{SS}) that is consistent with scattering particles of bicontinuous electron density. The results in terms of the sums of the $[Nb_6O_{19}]^{8-}$ core radius (R_S = 3.9 Å) and the shell thicknesses (owing to a combination of A^+ ions and associated water molecules) as represented schematically in Figure 1 d are presented in Table 2 and Figure 2 (right panel) as R_{SS} values. The average values of R_{SS} decrease from 7.6(7) Å for the five potassium ion system dilutions to 6.1(5) Å for the five rubidium ion system dilutions to 5.9(3) Å for the four cesium ion system dilutions. In as much as the last two values are statistically equivalent and are smaller than the value of the R_{SS} for the potassium ion system, this trend in the value of R_{SS} matches that of the radii of hydration of alkali metal ions, for which it is found that the radii are inversely proportional to the cation radius, that is, K > Rb > Cs (see Table 1). Thus, we propose that the large aggregates observed in the $K_8[Nb_6O_{19}]$/3 M KOH solutions consist, in part, of solvent ion pairs of hydrated potassium ions with $[Nb_6O_{19}]^{8-}$. A recent computational study by Poblet et al.[10] on the ion pairing of tungstate Keggin ions with alkali cations suggests that with smaller alkali cations, most ion interactions are solvent mediated, rather than being in direct contact as obtained for rubidium and cesium ions.

In this systematic SAXS investigation of the behavior of $[Nb_6O_{19}]^{8-}$ in aqueous alkaline solutions, the potassium, rubidium, and cesium salts have provided an ideal case study, owing to their high aqueous solubility and the high charge to surface-area ratio of the spherical anion. The combined results from calculation and experiments have provided direct insights into the topic of ion pairing. We have shown that the A^+ (A = K, Rb, Cs) associations with the $[Nb_6O_{19}]^{8-}$ anions observed in solid-state salts also prevail under selected solution conditions, and that contact ion pairing between A^+ and $[Nb_6O_{19}]^{8-}$ even persists when A^+ is not in great excess. Specifically, the comparison of the ion-pairing in 3 M TMAOH and 3 M AOH (A = K, Rb, Cs) media show contrasting behavior. On the one hand, in TMAOH solutions, in which the A^+ ions are dilute relative to the TMA cation, the bare $[Nb_6O_{19}]^{8-}$ ion predominates. At high anion concentrations, there is some contact ion-pairing with A^+ ions that cannot be quantified by the data. Solvent-shared ion pairing between hydrated A^+ and $[Nb_6O_{19}]^{8-}$ ions is not observed. On the other hand, in AOH solutions with A^+ ions in great excess, 8 A^+ cations directly contact or neutralize $[Nb_6O_{19}]^{8-}$ for A = Rb, Cs and 8–10 A^+ cations for A = K, which is in agreement with the geometry of $A_8^+[Nb_6O_{19}]^{8-}$ observed in the solid state (Figure 1 b and c).

The implications of these results concern separations science, wherein, for example, the removal of ^{137}Cs from alkaline high-level radioactive waste streams[32] may be accomplished using $[Nb_6O_{19}]^{8-}$ affixed to a surface. Furthermore, this system presents a rare opportunity for other spectroscopic observations of ion pairing in solution, such as by ^{133}Cs NMR spectroscopy. The electrostatic, contact ion-pairing interactions described herein are envisioned to occur prominently in other self- and directed-assembly processes as well, and the evidence of structural hierarchy in solution offers a glimpse into the incipient crystallization of a

molecular cluster. A high charge-to-size ratio of metal oxo polycations and polyanions is deemed responsible for ion-pairing applications, such as the optimized precipitation of contaminants from aqueous media.[19,33] In light of this ratio, Nb-POMs are very promising for such applications based on their unmatched high surface charge. However, the studies presented herein introduce a new caveat. Our results suggest that high charge is mitigated and neutralized by nonspecific ion association, such as with alkali metal ions or protons, which render the highly charged species less accessible to more selective ion pairing, such as with a charged biomolecule. Thus exploitation of high surface charge for specific ion pairing and precipitation in aqueous media is not necessarily accomplished by the highest-charged species, but rather by those charged species that are stable without protonation, deprotonation, or nonspecific ion association.

Experimental Section

The Lindqvist ion salts $K_8[Nb_6O_{19}]\cdot 16H_2O$, $Rb_8[Nb_6O_{19}]\cdot 14H_2O$, and $Cs_8[Nb_6O_{19}]\cdot 16H_2O$ were synthesized as previously described.[26] Solutions of each salt were prepared for a variety of concentrations ranging from 0.56 to circa 1000 mM in 3 M TMAOH solution and 3 M AOH solutions (A = K, Rb) and contained in a 2 mm diameter quartz capillary tubes for SAXS measurements, except for the solutions of $Cs_8[Nb_6O_{19}]\cdot 16H_2O$ in 3 M CsOH, which were contained in 1.5 mm diameter quartz capillary tubes. The high concentration of base ensured monospecific solutions without protonation of the Lindqvist clusters. The solution concentrations are summarized Table 1. The atomic scattering intensities, $I_a(Q)$ in vacuo, were calculated from the crystallographically-determined atomic coordinates for the hexaniobate anion, $[Nb_6O_{19}]^{8-}$, its neutral clusters, $A_8[Nb_6O_{19}]$ (A = K, Rb, Cs) and the charged species $K_4[Nb_6O_{19}]^{4-}$, $K_{10}[Nb_6O_{19}]^{2+}$, and the TMA cation[34] by use of CRYSOL.[35] The calculated $I_a(Q)$ vs. Q for $0.005 \le Q \le 1.0$ Å^{-1} are shown in the Supporting Information (Figure S1), and the calculated R_g values are provided in Table 2.

Small-angle X-ray scattering data were collected at beam line 12-BM-B of the Advanced Photon Source at Argonne National Laboratory.[36] An incident photon energy of 15.0 keV, which is below the K-edge energies of Rb and Nb (15.2 and 18.986 keV, respectively) and high above the K-edge energy of K (3.608 keV), was chosen to provide good X-ray transmittance for all dilutions, except those in 3 M CsOH. Because of the highly absorbing nature of the 3 M CsOH media, a higher incident energy, 20.314 keV, in combination with a smaller diameter capillary tube were used (to reduce absorption) for data acquisition. The 2D scattering profiles were recorded at ambient temperature with a MAR-CCD-165 detector, which has a circular, 165 mm diameter active area and 2048×2048 pixel resolution. The sample-to-detector distance was adjusted to provide a detecting range for momentum transfer of $0.03 \le Q \le 1.0$ Å^{-1}. The scattering vector Q was calibrated using a silver behenate standard.[37] After correction for spatial distortion and detector sensitivity, the 2D scattering images were radially averaged to produce plots of scattered intensity, $I(Q)$ vs. Q, where $Q = 4\pi\sin\theta\lambda$ (Å^{-1}), in which 2θ is the scattering angle and λ is the wavelength of the X-rays, following standard procedures.[38] The primary, background-subtracted SAXS data for the dilute solutions of 0.56–55.6 mM (Table 1) of the Lindqvist salts in the 3 M AOH and TMAOH media are shown in the Supporting Information (Figure S2 and S3).

Guinier analysis of the background-subtracted $I(Q)$ data in the low Q region provided the radii of gyration, R_g (Table 2) for the molecular anions. R_g is obtained from the Guinier plots $\ln(I(Q))$ vs. Q^2, (Supporting Information, Figure S2 and S3) by use of conventional methods.[38,39] The Guinier plots show linear and parallel behavior that is independent of concentration, which is typical of monodisperse systems without complications from interparticle effects. In addition, the values of $I(Q)$ extrapolated to $Q = 0$ Å^{-1} (I_0) as obtained from the Guinier fits scale directly and linearly with concentration (Supporting Information, Figure S4 and S5), a response which further confirms that the anions are free from interparticle effects. The distance distribution functions, $p(r)$ vs. r, where $p(r)$ is the probability of finding the vector length r in the molecule that will become zero at the maximum vector length, were obtained from the fits to the $I(Q)$ data using the inverse Fourier transform (FT) method of Moore.[40] All distance distribution plots (Supplementary information, Figure S6) show single, symmetric peaks with maximum dimensions corresponding to either the bare Lindqvist anion (8.3(1) Å), as measured by the average of three terminal O–O interatomic distances across each of the three orthogonal axes through the cluster, or to the $8A^+$-decorated systems (9.4–10.0 Å), as measured by twice the average distances between the central oxygen atom and the A^+ ions attached by three bridging oxygen atoms for the $K_8[Nb_6O_{19}]$, $Rb_8[Nb_6O_{19}]$, and $Cs_8[Nb_6O_{19}]$ cation–anion associated species in the solid state, as illustrated in Figure 1. The inverse FT fits to the $I(Q)$ vs. Q data also provide an independent measure of the system of R_g values, which are equivalent to those obtained from the classical Guinier analyses.

Received: October 31, 2008
Published online: April 24, 2009

Keywords: alkali metals · cluster compounds · ion pairs · polyoxometalates · small-angle X-ray scattering

[1] R. Billing, D. Rehorek, H. Hennig, *Top. Curr. Chem.* **1990**, *158*, 151.
[2] V. A. Grigoriev, D. Cheng, C. L. Hill, I. A. Weinstock, *J. Am. Chem. Soc.* **2001**, *123*, 5292.
[3] R. J. Forster, L. R. Faulkner, *J. Am. Chem. Soc.* **1994**, *116*, 5444.
[4] M. J. Han, Y. M. Chen, K. Z. Wang, *New J. Chem.* **2008**, *32*, 970.
[5] M. R. Sambrook, P. D. Beer, J. A. Wisner, R. L. Paul, A. R. Cowley, F. Szemes, M. G. B. Drew, *J. Am. Chem. Soc.* **2005**, *127*, 2292.
[6] M. O. de la Cruz, L. Belloni, M. Delsanti, J. P. Dalbiez, O. Spalla, M. Drifford, *J. Chem. Phys.* **1995**, *103*, 5781.
[7] C. Schmuck, *Coord. Chem. Rev.* **2006**, *250*, 3053.
[8] J. D. Meyer, M. C. Manning, *Pharm. Res.* **1998**, *15*, 188.
[9] M. Xu, J. P. Larentzos, M. Roshdy, L. J. Criscenti, H. C. Allen, *Phys. Chem. Chem. Phys.* **2008**, *10*, 4793.
[10] F. Leroy, P. Miro, J. M. Poblet, C. Bo, J. B. Avalos, *J. Phys. Chem. B* **2008**, *112*, 8591.
[11] T. M. Anderson, C. L. Hill, *Inorg. Chem.* **2002**, *41*, 4252.
[12] M. L. Kistler, A. Bhatt, G. Liu, D. Casa, T. B. Liu, *J. Am. Chem. Soc.* **2007**, *129*, 6453.
[13] D. Volkmer, A. DuChesne, D. G. Kurth, H. Schnablegger, P. Lehmann, M. J. Koop, A. Muller, *J. Am. Chem. Soc.* **2000**, *122*, 1995.
[14] C. L. Hill, *J. Mol. Catal. A* **2007**, *262*, 2.
[15] Y. Marcus, G. Hefter, *Chem. Rev.* **2006**, *106*, 4585.
[16] A. Goiffon, E. Philippote, M. Maurin, *Rev. Chim. Miner.* **1980**, *17*, 466.
[17] I. Lindqvist, *Ark. Kemi* **1953**, *5*, 247.
[18] In view of its spherical morphology with a radius of 4.0 Å, the surface charge on $[Nb_6O_{19}]^{8-}$ is calculated as -3.98×10^{-2} Å^{-2}. By comparison, the 53-atom, spherical Keggin POM, $[PW_{12}O_{40}]^{3-}$ with a radius of 5.1 Å, and the 146-atom oblate ellipsoid, Preyssler POM $[NaP_5W_{30}O_{110}]^{14-}$ with $r_{maj} = 7.4$ Å and $r_{min} = 5.1$ Å, have surface charges of -9.18×10^{-3} Å^{-2} and -2.54×10^{-2} Å^{-2}, respectively; see Ref. [39].

[19] I. S. Lee, J. R. Long, S. B. Prusiner, J. G. Safar, *J. Am. Chem. Soc.* **2005**, *127*, 13802.
[20] M. Nyman, F. Bonhomme, T. M. Alam, M. A. Rodriguez, B. R. Cherry, J. L. Krumhansl, T. M. Nenoff, A. M. Sattler, *Science* **2002**, *297*, 996.
[21] J. R. Black, M. Nyman, W. H. Casey, *J. Am. Chem. Soc.* **2006**, *128*, 14712.
[22] M. Nyman, A. J. Celestian, J. B. Parise, G. P. Holland, T. M. Alam, *Inorg. Chem.* **2006**, *45*, 1043.
[23] M. Nyman, J. P. Larentzos, E. J. Maginn, M. E. Welk, D. Ingersoll, H. Park, J. B. Parise, I. Bull, F. Bonhomme, *Inorg. Chem.* **2007**, *46*, 2067.
[24] T. M. Anderson, M. A. Rodriguez, F. Bonhomme, J. Bixler, T. M. Alam, M. Nyman, *Dalton Trans.* **2007**, 4517.
[25] T. M. Anderson, S. G. Thoma, F. Bonhomme, M. A. Rodriguez, H. Park, J. B. Parise, T. M. Alam, J. P. Larentzos, M. Nyman, *Cryst. Growth Des.* **2007**, *7*, 719.
[26] M. Nyman, T. M. Alam, F. Bonhomme, M. A. Rodriguez, C. S. Frazer, M. E. Welk, *J. Cluster Sci.* **2006**, *17*, 197.
[27] M. T. Pope, *Heteropoly and Isopoly Oxometalates*, Springer, Berlin, **1983**.
[28] C. D. Putnam, M. Hammel, G. L. Hura, J. A. Tainer, *Q. Rev. Biophys.* **2007**, *40*, 191.
[29] Y. Marcus, *Ion Properties*, Marcel Dekker, New York, **1997**.
[30] O. Glatter, R. May in *Mathematical, Physical and Chemical Tables*, *Vol. C*: *International Tables for Crystallography*, 2nd ed (Eds. A. J. C. Wilson and E. Prince), Springer, Dordrecht, **1999**, 89.
[31] R. D. Shannon, *Acta Crystallogr. Sect. A* **1976**, *32*, 751.
[32] P. V. Bonnesen, L. H. Delmau, B. A. Moyer, G. J. Lumetta, *Solvent Extr. Ion Exch.* **2003**, *21*, 141.
[33] M. Q. Yan, D. S. Wang, J. H. Qu, W. J. He, C. W. K. Chow, *J. Colloid Interface Sci.* **2007**, *316*, 482.
[34] D. Mootz, R. Seidel, *J. Inclusion Phenom. Mol. Recognit. Chem.* **1990**, *8*, 139.
[35] D. Svergun, C. Barberato, M. H. J. Koch, *J. Appl. Crystallogr.* **1995**, *28*, 768.
[36] S. Seifert, R. E. Winans, D. M. Tiede, P. Thiyagarajan, *J. Appl. Crystallogr.* **2000**, *33*, 782.
[37] U. Keiderling, R. Gilles, A. Wiedenmann, *J. Appl. Crystallogr.* **1999**, *32*, 456.
[38] A. Guinier, G. Fournet, *Small-Angle Scattering of X-rays*, Wiley, New York, **1955**.
[39] M. R. Antonio, M. H. Chiang, S. Seifert, D. M. Tiede, P. Thiyagarajan, *J. Electroanal. Chem.* **2009**, *626*, 103.
[40] P. B. Moore, *J. Appl. Crystallogr.* **1980**, *13*, 168.

